Phase shift approximation for the post-critical seismic wave

2012 J. Geophys. Eng. 9 482

(http://iopscience.iop.org/1742-2140/9/5/482)

IOP Publishing Journal of Geophysics and Engineering
J. Geophys. Eng. **9** (2012) 482–493 doi:10.1088/1742-2132/9/5/482

Phase shift approximation for the post-critical seismic wave

Xinyan Zhang[1], Zhongjie Zhang[1], Tao Xu[1], Zhiming Bai[1] and Jerry M Harris[2]

[1] State Key Laboratory of Lithospheric Evolution, Institute of Geology and Geophysics, Chinese Academy of Sciences, Beijing, 100029, People's Republic of China
[2] Department of Geophysics, Stanford University, Stanford, CA 94305-2215, USA

E-mail: zhangxinyan@mail.iggcas.ac.cn

Received 23 April 2012
Accepted for publication 9 July 2012
Published 16 August 2012
Online at stacks.iop.org/JGE/9/482

Abstract
Post-critical seismic waves are widely used in crustal exploration of the seismic velocity structure, and are gaining interest in the oil/gas seismic community to image the deeper structure beneath the high velocity basalt layer. They are featured with their phase shifts and strength changes, which should be taken into account in seismic data processing, such as velocity analysis and true amplitude migration, etc. In order to simplify the exact but complicated formula of reflection and transmission coefficients, numerous approximate expressions for reflection and transmission coefficients for pre-critical incidence are obtained. In the post-critical case, there is Downton's approximation with acceptable accuracy approximation when the velocity changes smoothly. However if the velocity model changes rapidly, the error will be relatively very large, limiting the use of the approach. In order to improve the post-critical approximation, we utilize Taylor expansion of ray parameters with angle increment (compared to critical angle) in wide-angle seismic reflection and transmission coefficients. The explicit expressions for amplitude and phase shift (time shift) for the post-critical incident angle are obtained. Our results confirm that the wide-angle seismic reflection/transmission phase shifts are strongly frequency dependent; phase shifts of low frequency wide-angle seismic waves are more predominant and their correction should be considered in seismic processing and imaging. Numerical examples demonstrate that (1) the accuracies of these approximations are high compared to the classic Aki's formula and Downton's approximation, and (2) the wide-angle effect can be effectively reduced with phase-shift correction by utilizing our time-shift approximation to the seismic traveltimes.

Keywords: wide-angle seismic reflection/transmission, post-critical angle, amplitude, phase shift, time shift

(Some figures may appear in colour only in the online journal)

1. Introduction

Wide-angle seismic waves result from post-critical angle incidence at underground discontinuities, and are featured with strong reflections which are easy to recognize in shot gathers, especially traveltime-reduced shot gathers of deep seismic sounding experiments (Li and Mooney 1998, Zhang *et al* 2011a). Wide-angle seismic profiling has been widely used to explore the deep crustal structure since the 1950s (Oliver and Coggon 1976). These waves are also used in the oil/gas industry as they can penetrate below the high velocity basalt barrier layer formed from intrusive and extrusive lavas (covering large areas of the earth) (Pramanik *et al* 2001). In the use of wide-angle reflection/transmission seismic waves, we need to correct for the corresponding phase shift and amplitude change from post-critical angle

incidence (Aki and Richards 1980). Neglecting this phase-shift correction in wide-angle seismic profiling (whether in a deep crustal structure or in oil/gas exploration with high velocity overburden) will lead to errors both of objective reflector depths and interval velocities. Usually, we call this phenomenon the post-critical effect. The comparison with CDP reflection images demonstrates that there is about 1–2 km crustal thickness (Moho depth) difference between vertical seismic reflection profiling and wide-angle seismic profiling (Zhang *et al* 2000). This difference is usually attributed to the phase picking uncertainties of intra-crustal reflections (including Moho reflection event PmP) (Oueity and Clowes 2010). Actually the phase shift (time shift) of wide-angle intra-crustal reflections compared to near vertical CDP reflections can be an alternative candidate to explain this difference. Obtaining a formula for wide-angle seismic phase shift is the basis to correct for the post-critical effect on seismic imaging. Reflection/transmission coefficients (R/T coefficients) can be calculated with exact mathematical expressions (Aki and Richards 1980), but they are complicated. The complication has led seismologists to derive approximate formulae appropriate to seismic applications (Bortfeld 1961, Richards and Frasier 1976, Wiggins *et al* 1984, Shuey 1985, Ursenbach 2003a, 2003b, Wang 1999). Summarizing the approximations above, they are almost performed on the condition that the incident angle is small and below the critical angle. As a result of improvements in acquisition quality and longer spread lengths, there is interest in analysing amplitude and time-shift behaviour up to and even beyond the critical angle. We can expect a similar approximation of R/T coefficients with post-critical angle incidence, which can be effectively used in oil/gas exploration and crustal structure (especially in the case of lower impendence contrast). Based on Aki and Richards's linearized approximation of PP reflection coefficient $R(\theta)$, Downton put forward an alternative method to deal with post-critical R/T coefficients. When the incident angle was beyond the critical angle, he mathematically expressed the transmitted angle as a complex number and substituted the average of incident and transmitted angles for the incident angle (Downton and Ursenbach 2006). The accuracy of his approach can be accepted for a small jump in velocity, but if the velocity model changes rapidly, the error is so large that the approach cannot be used.

The paper is arranged in this way: firstly, Taylor expansion of ray parameter and horizontal slowness with angle increment (compared to critical angle) is used in wide-angle seismic reflection and transmission coefficients, and then the explicit expressions for amplitude and phase shift are obtained. In order to show the high precision of our approximation formulae, we present the comparison of calculated amplitude and phase shift among exact coefficient formulae (Aki and Richards 1980), Downton's alternative method (Downton and Ursenbach 2006) and our approximate formulae. We also discuss the phase shift and its correction for synthetic wide-angle reflections from Moho discontinuity with one crustal model in China mainland. Lastly, we present brief concluding remarks.

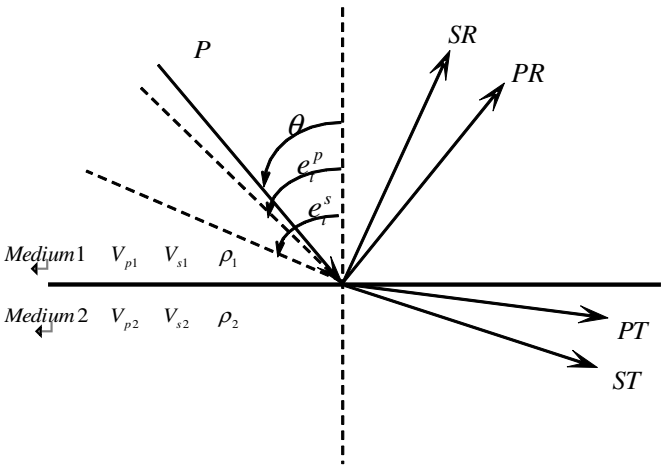

Figure 1. A flat interface separating two isotropic media. The elastic coefficients for the upper and lower media are shown in the figure.

2. Approximations of R/T coefficients and their phase shifts

Consider a flat interface separating two isotropic media (figure 1). A plane P wave incident on the planar interface can generally generate four waves—a reflected P wave, a reflected S wave, a transmitted P wave and a transmitted S wave.

The exact formulae for all the R/T coefficients are as follows (Aki and Richards 1980) (R_{PP} and R_{PS} are the reflection coefficients of the reflected PP and PS waves; T_{PP} and T_{PS} are the transmission coefficients of the transmitted PP and PS waves, respectively):

$$R_{PP}(p) = \frac{E + Fp^2 + Gp^4 - Dp^6}{A + Bp^2 + Cp^4 + Dp^6}, \tag{1a}$$

$$T_{PP}(p) = \frac{H + Ip^2}{A + Bp^2 + Cp^4 + Dp^6}, \tag{1b}$$

$$R_{PS}(p) = \left(2q_{a1}\frac{V_{p1}}{V_{s1}}p\right)\frac{J + Kp^2 - Dp^4}{A + Bp^2 + Cp^4 + Dp^6}, \tag{1c}$$

$$T_{PS}(p) = \left(2q_{a1}\frac{V_{p1}}{V_{s2}}p\right)\frac{L + Mp^2}{A + Bp^2 + Cp^4 + Dp^6}, \tag{1d}$$

where

$$A = (\rho_2 q_{a1} + \rho_1 q_{a2})(\rho_2 q_{b1} + \rho_1 q_{b2}), \tag{1e}$$

$$B = -4\Delta\mu(\rho_2 q_{a1} q_{b1} - \rho_1 q_{a2} q_{b2}) + (\Delta\rho)^2 + 4(\Delta\mu)^2 q_{a1} q_{a2} q_{b1} q_{b2}, \tag{1f}$$

$$C = 4(\Delta\mu)^2(q_{a1} q_{b1} + q_{a2} q_{b2}) - 4\Delta\mu\Delta\rho, \tag{1g}$$

$$D = 4(\Delta\mu)^2, \tag{1h}$$

$$E = (\rho_2 q_{a1} - \rho_1 q_{a2})(\rho_2 q_{b1} + \rho_1 q_{b2}), \tag{1i}$$

$$F = -4\Delta\mu(\rho_2 q_{a1} q_{b1} + \rho_1 q_{a2} q_{b2}) - (\Delta\rho)^2 + 4(\Delta\mu)^2 q_{a1} q_{a2} q_{b1} q_{b2}, \tag{1j}$$

$$G = 4(\Delta\mu)^2(q_{a1} q_{b1} - q_{a2} q_{b2}) + 4\Delta\mu\Delta\rho, \tag{1k}$$

$$H = 2(\rho_2 q_{b1} + \rho_1 q_{b2})\rho_1 q_{a1}(V_{p1}/V_{p2}), \tag{1l}$$

$$I = -4\Delta\mu(q_{b1} - q_{b2})\rho_1 q_{a1}(V_{p1}/V_{p2}), \tag{1m}$$

$$J = -\rho_2\Delta\rho - 2\rho_1 q_{a2} q_{b2}\Delta\mu, \tag{1n}$$

$$K = 2(\rho_2 + \Delta\rho)\Delta\mu - 4q_{a2}q_{b2}(\Delta\mu)^2, \tag{1o}$$

$$L = \rho_1\Delta\rho - 2\rho_1 q_{a2} q_{b1}\Delta\mu, \tag{1p}$$

$$M = -2\rho_1\Delta\mu, \tag{1q}$$

with

$$q_{a1} = \sqrt{1/V_{p1}^2 - p^2}, \tag{1r}$$

$$q_{a2} = \sqrt{1/V_{p2}^2 - p^2}, \tag{1s}$$

$$q_{b1} = \sqrt{1/V_{s1}^2 - p^2}, \tag{1t}$$

$$q_{b2} = \sqrt{1/V_{s2}^2 - p^2}, \tag{1u}$$

$$\Delta\rho = \rho_2 - \rho_1, \tag{1v}$$

$$\Delta\mu = \rho_2 V_{s2}^2 - \rho_1 V_{s1}^2. \tag{1w}$$

In the above equations, the parameter p is the 'ray parameter', or the 'horizontal slowness', and is related to the incident angle θ; the quantities q_{a1}, q_{a2}, q_{b1}, q_{b2} are called the 'vertical slowness' of the reflected PP wave, reflected PS wave, transmitted PP wave and transmitted PS wave, respectively; V_{p1}, V_{p2}, V_{s1} and V_{s2} are the P-wave and S-wave velocities of the upper and lower media, respectively; ρ_1 and ρ_2 are the densities; μ_1 and μ_2 are the shear moduli; $\Delta\rho$ is the density difference and $\Delta\mu$ is the shear modulus difference between the two media.

For seismic waves on discontinuity in an elastic medium, there are two kinds of critical angles, PP wave critical angle and PS wave critical angle:

(1) $e_c^p = \sin^{-1}\left(\frac{V_{p1}}{V_{p2}}\right)$, for a transmissive PP wave when $V_{p1} < V_{p2}$;
(2) $e_c^s = \sin^{-1}\left(\frac{V_{p1}}{V_{s2}}\right)$, for a transmissive PS wave when $V_{p1} < V_{s2}$.

Practically, it is common to consider PP wave critical angle in a large-aperture seismic experiment. However, the condition $V_{p1} < V_{s2}$ is invalid in common situations, although in deep crustal experiments, the second situation can occur. For example, shear heating and other potential mechanisms can reduce P-wave velocity by 10%, but keep S-wave velocity with no change, as demonstrated by physical experiments (Carpenter 2006). Another possibility is from oceanic plate subduction, where sediment can subduct with solid lithosphere to form a strength discontinuity between the sediment with P-wave velocity V_{p1} and the solid subducted plate with higher S-wave velocity V_{s2}.

If the incident angle θ is larger than the critical angle, that is $\theta > e_c^p$, q_{a2} becomes complex. The post-critical coefficients, R_{PP}, R_{PS}, T_{PP} and T_{PS}, also become complex. Complex numbers are used to contain the phase information. That is to say, the traveltimes of PP and PS waves are featured by post-critical phase shifts (time shifts).

In the following, we derive the approximate expression for the phase shift. With the similarity of the derivation process, we just take the P-P reflection coefficient R_{PP} as an example.

Corresponding to the above-mentioned two critical angles, we discuss the phase shift approximation in two situations.

- Situation 1: $e_c^p < \theta < e_c^s$.
- Situation 2: $e_c^s < \theta < \frac{\pi}{2}$.

The above two cases are analysed mathematically, in order to keep the vertical slowness real. For the ray parameter and horizontal slowness, we use fourth-order Taylor expansion respectively at the points e_c^p and e_c^s, corresponding to situations 1 and 2:

$$\begin{aligned} p &= \delta_1 + \delta_2(\Delta\theta) + \delta_3(\Delta\theta)^2 + \delta_4(\Delta\theta)^3 + \delta_5(\Delta\theta)^4, \\ p^2 &= \alpha_1 + \alpha_2(\Delta\theta) + \alpha_3(\Delta\theta)^2 + \alpha_4(\Delta\theta)^3 + \alpha_5(\Delta\theta)^4, \\ p^4 &= \beta_1 + \beta_2(\Delta\theta) + \beta_3(\Delta\theta)^2 + \beta_4(\Delta\theta)^3 + \beta_5(\Delta\theta)^4, \\ p^6 &= \gamma_1 + \gamma_2(\Delta\theta) + \gamma_3(\Delta\theta)^2 + \gamma_4(\Delta\theta)^3 + \gamma_5(\Delta\theta)^4, \end{aligned} \tag{2a}$$

$$\begin{aligned} q_{a1} &= A_0 + B_0(\Delta\theta) + C_0(\Delta\theta)^2 + D_0(\Delta\theta)^3 + E_0(\Delta\theta)^4, \\ q_{b1} &= A_1 + B_1(\Delta\theta) + C_1(\Delta\theta)^2 + D_1(\Delta\theta)^3 + E_1(\Delta\theta)^4, \end{aligned} \tag{2b}$$

and

$$\begin{aligned} q_{b2} &= A_2 + B_2(\Delta\theta) + C_2(\Delta\theta)^2 + D_2(\Delta\theta)^3 + E_2(\Delta\theta)^4, \\ q_{a2} &= \mathrm{i}\sqrt{A_3 + B_3(\Delta\theta) + C_3(\Delta\theta)^2 + D_3(\Delta\theta)^3 + E_3(\Delta\theta)^4}, \end{aligned} \tag{2c}$$

$\Delta\theta = \theta - e_c^p$, for situation 1;

$$\begin{aligned} q_{a2} &= \mathrm{i}\sqrt{A_2 + B_2(\Delta\theta) + C_2(\Delta\theta)^2 + D_2(\Delta\theta)^3 + E_2(\Delta\theta)^4}, \\ q_{b2} &= \mathrm{i}\sqrt{A_3 + B_3(\Delta\theta) + C_3(\Delta\theta)^2 + D_3(\Delta\theta)^3 + E_3(\Delta\theta)^4}, \end{aligned} \tag{2d}$$

$\Delta\theta = \theta - e_c^s$, for situation 2.

The corresponding parameters δ_1–δ_5, α_1–α_5, β_1–β_5, γ_1–γ_5, A_0–E_0, A_1–E_1, A_2–E_2, A_3–E_3 are shown in appendices A and B respectively for situations 1 and 2.

The strength and phase shift for a reflective PP wave for post-critical incidence can be approximated in the following form after substituting equations (2*a*)–(2*d*) into equation (1*a*):

$$|R_{PP}(\theta)| = \frac{\sqrt{(U_1O_1 + U_2O_2)^2 + (U_2O_1 - U_1O_2)^2}}{O_1^2 + O_2^2}, \tag{3a}$$

$$\varphi(\theta) = \arctan\left(\frac{U_2O_1 - U_1O_2}{U_1O_1 + U_2O_2}\right). \tag{3b}$$

If the frequency of the incident seismic wave is f, then the time shift is

$$\Delta t = \frac{\varphi}{2\pi f}. \tag{3c}$$

Expressions for U_1, U_2, O_1 and O_2 are shown in appendices A and B, corresponding to situations 1 and 2.

Similar to the derivation of R_{PP}, approximations to R_{PS}, T_{PP} and T_{PS} can be performed in the same way, and the corresponding results can be seen in appendix C.

3. Numerical evaluation of wide-angle seismic reflection strength and phase shift approximation

To demonstrate the accuracy of the approximation above, we designed a model with two layers of media and one flat boundary between them, and the related parameters to describe the model can be seen in table 1. With this model,

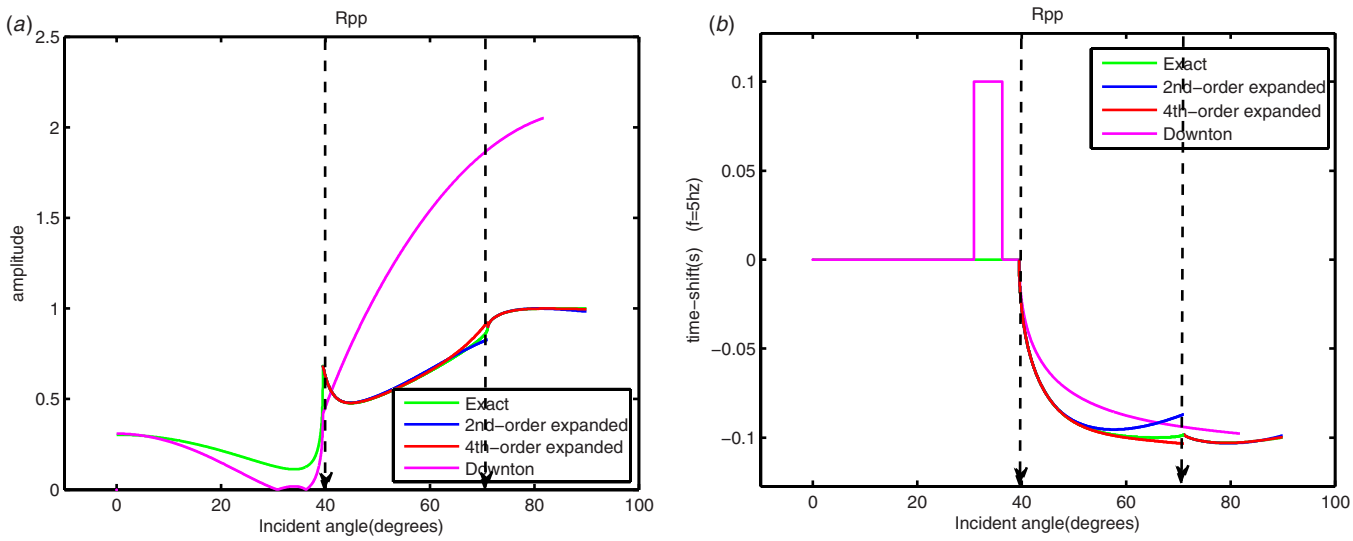

Figure 2. (*a*) Amplitude of R_{PP}; (*b*) time shift of R_{PP} with a frequency of 5 Hz. Comparison of the different approximations for the amplitude and time shift of the P-P wave reflection coefficient. The exact results cover the range of incident angle from 0° to 90°, as do Downton's results also, and ours are from the first critical angle to 90°. The broken lines in the figure show the position of the two critical angles.

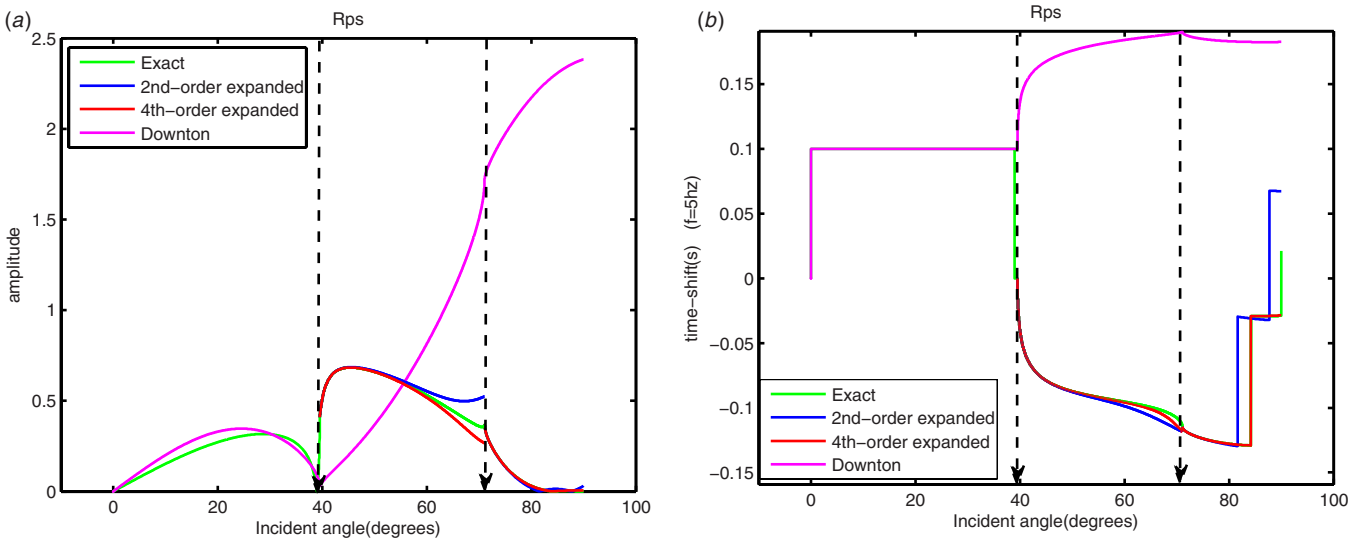

Figure 3. Same as figure 2 but for the P-S wave reflection coefficient R_{PS}.

Table 1. Elastic parameters for a two-layer model.

Medium	V_p (km s^{-1})	V_s (km s^{-1})	ρ (kg m^{-3})
1	3500	2020	2.10
2	5500	3700	2.5

we calculated (1) their theoretical expectations with the classic formula (Aki and Richards 1980), and the approximate results of the reflection coefficient and phase shift with (2) Downton's scheme (Downton and Ursenbach 2006) and (3) our approximation formula in equations (3*a*)–(3*c*). Figure 2 presents comparisons of amplitude and time shift (with the wave frequency of 5 Hz) of R_{PP} in this model. With $V_{p1} < V_{s2}$ in this model, we can observe that the reflection strength increases abruptly at PP critical angle and PS critical angle. This strong PS reflection at PS post-critical angle can be used to explain bright point PS reflection observation in the INDEPTH-II wide-angle seismic experiment (an international deep profiling of the Himalayas and Tibetan plateau, carried out during 1994–1995) (Makovsky *et al* 1996). For the comparison, the exact results cover the domain of incident angle from 0° to 90°, as do Downton's results also, and ours is from the first critical angle (PP critical angle) to 90° (for we are only absorbed in the post-critical R/T coefficients). Taking the PP reflection coefficient for example (figures 2(*a*) and (*b*)), we can observe that (1) strength and time shift calculated in Downton's method fit well with theoretical values when the incident angle is less than the critical angle, but there is large error when the incident angle is larger than the critical angle. For the strength (figure 2(*a*)), Downton's result increases rapidly with the incident angle, much larger than the theoretical result, and when it is beyond the second critical angle (PS critical angle), the error of strength even exceeds 200%. Such low accuracy cannot be accepted. For the time shift (figure 2(*b*)), it is shown that there is

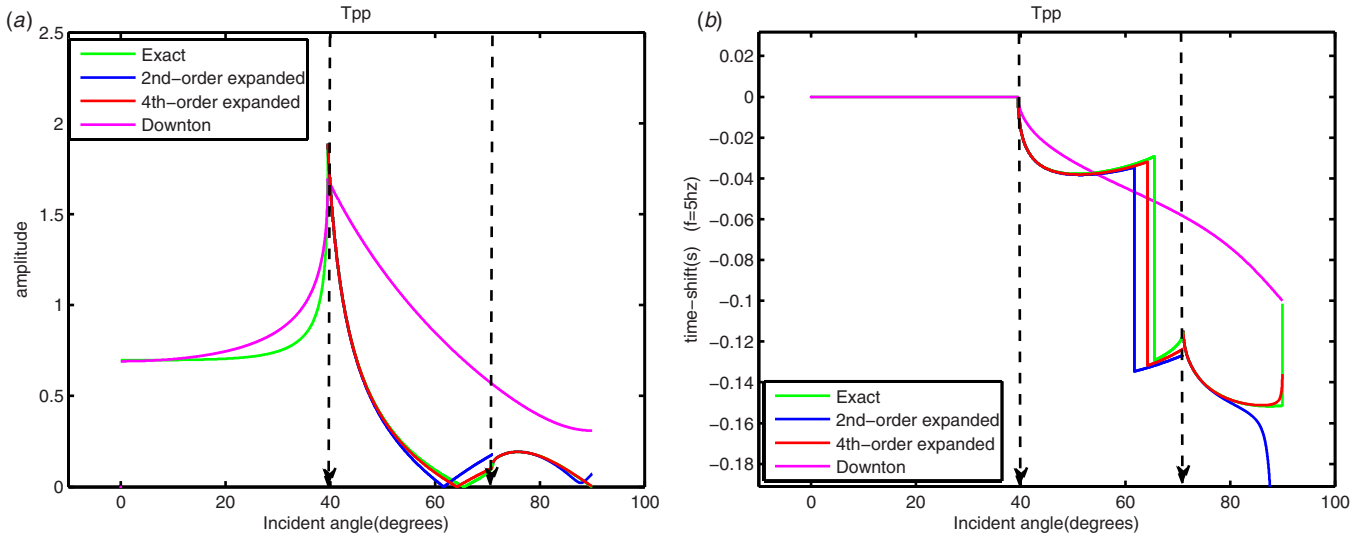

Figure 4. Same as figure 2 but for the P-P wave transmission coefficient T_{PP}.

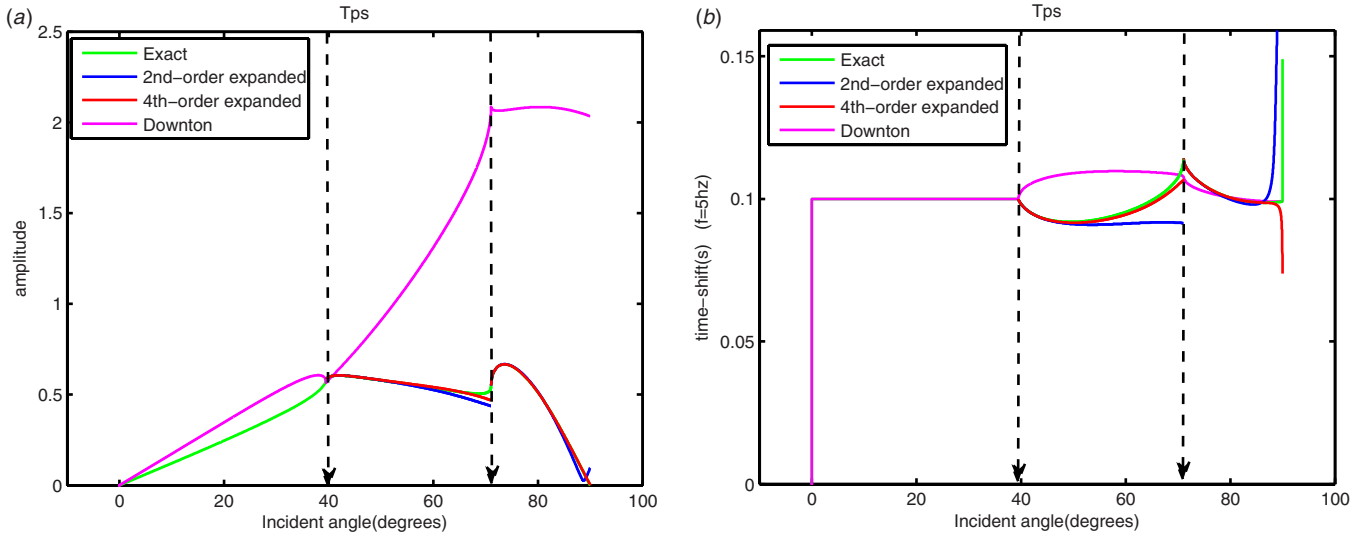

Figure 5. Same as figure 2 but for the P-S wave transmission coefficient T_{PS}.

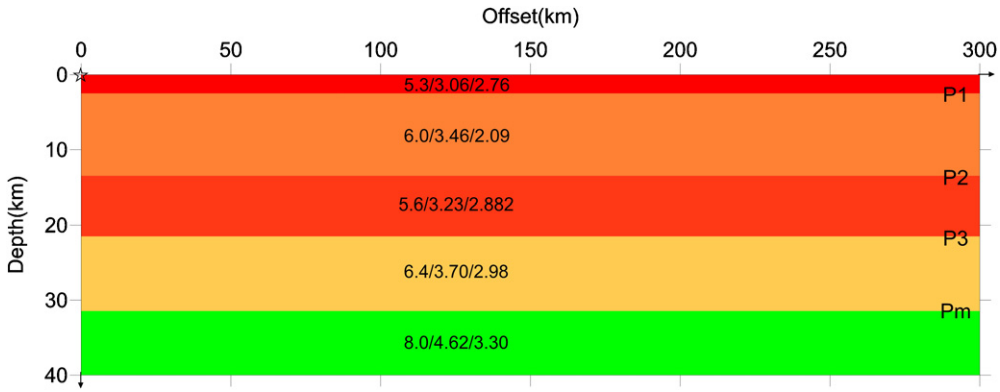

Figure 6. A crustal structure. Layer thickness, P- and S-wave velocities and density parameters are shown in the figure. The model consists of five layers, with the top (first) layer as sediment, and the interface at a depth of 32 km is the Moho discontinuity between the crust and the upper mantle. The source is placed at the surface, and the observational system is deployed to record the seismic signal. The maximum offset is 300 km.

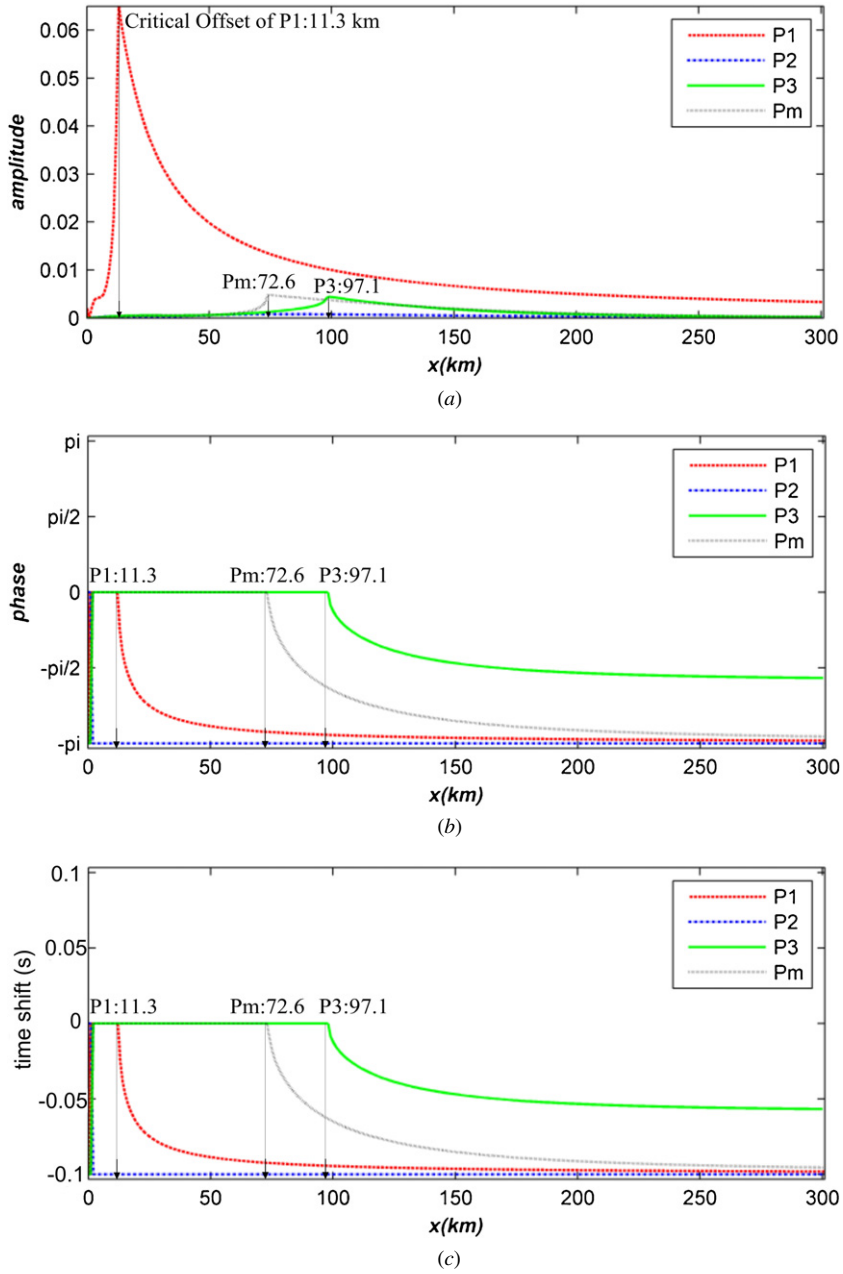

Figure 7. The horizontal components of effective amplitude (*a*), phase shift (*b*) and time shift (*c*) for each seismic phase. The reflection strength (amplitude), phase and time increase abruptly when the offset is 11.3, 72.6 and 97.1 km, respectively, for P1, P3 and Pm, as marked in the figure.

time delay in the post-critical case, which becomes larger with the increase of incident angle. Compared to the theoretical time delay, Downton's is much smaller with the error remaining up to 15%. (2) At the post-critical incident angle, wide-angle seismic reflection strength and time shift calculated with our approximation formula match well with theoretical curves, with the error remaining lower than 5%. The relationship between reflection strength, phase shift and incidence angle (>critical angle) with our approximate formula is well kept as the theoretical expectation. These results suggest that the accuracies of our approximations from second- and fourth-order Taylor expansions are acceptable. The comparisons for R_{PS}, T_{PP} and T_{PS} as respectively shown in figures 3–5 can produce similar conclusions of high approximation accuracy to that about the PP reflection strength/phase shift.

4. Synthetic seismograms and effect of wide-angle phase shift

In the following, we collect a crustal structure model to evaluate the effect of wide-angle phase shift on a wide-angle seismic experiment (figure 6). The model is the average crustal velocity structure of North China craton in China continent (Li and Mooney 1998, Zhang *et al* 2011b). The crustal structure, layer thickness, P- and S-wave velocities and density parameters are shown in figure 6. The model consists of five

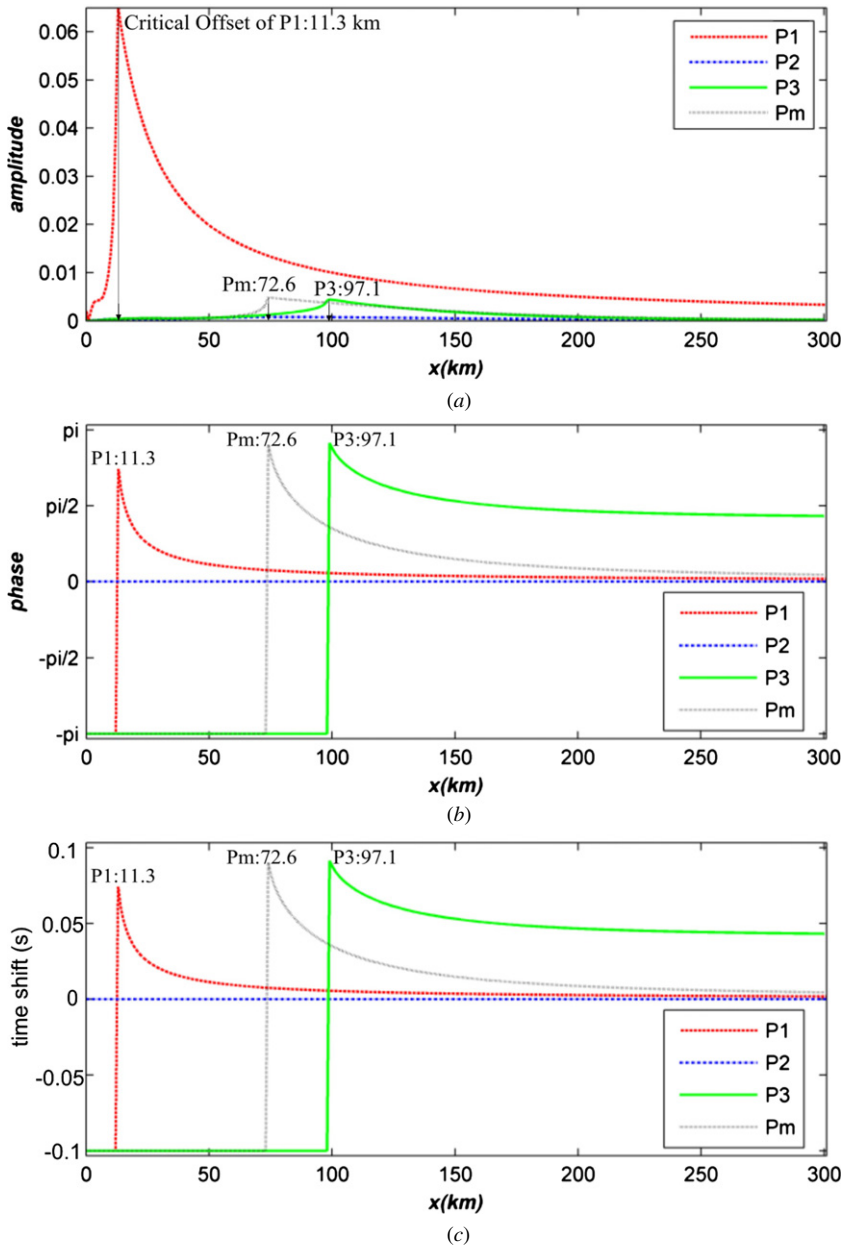

Figure 8. Same as figure 7, but for vertical components.

layers, with the top (first) layer as sediment, and the interface at a depth of 32 km is the Moho discontinuity between the crust and the upper mantle. The source is placed at the surface, and a two-side observational system is deployed to record the seismic signal. The maximum offset is 300 km. From this velocity model, the critical angle for the reflection P1 from the sediment bottom is 62.08°, the critical angle for the reflection P3 from the third interface is 61.08° and the critical angle for the reflection Pm from the Moho is 53.16°. Since the third layer is a low velocity layer, there is no seismic reflection with the post-critical angle incidence from interface P2.

Then, the amplitude and phase shift (time shift) of wide-angle seismic reflections from each interface (figures 7(*a*)–(*c*) and 8(*a*)–(*c*)) were calculated on horizontal- and vertical-component seismic gathers. We can observe that both the reflection strength (amplitude) and phase increase abruptly when the offset is 11.3, 72.6 and 97.1 km respectively for the reflections P1, P3 and Pm.

Synthetic seismograms were calculated with finite-difference code (Virieux 1984, Lan and Zhang 2011a, 2011b). In the calculation, the predominant frequency of the seismic source is 5 Hz. Figures 9 and 10 display seismic records of horizontal and vertical components, respectively. With these synthetic seismograms, we can observe several seismic events, such as the reflections from (1) the bottom of the sediment, (2) the Moho interface and (3) other intra-crustal interfaces. The real curves on seismic gathers are the pick-up of these reflection events (with picked travel-times Tp). We regard Tp as the exact travel-time of these seismic events (which may include the wide-angle effect from full wave equation modelling for discussion). In order to evaluate the phase shift effect of wide-angle seismic reflections, we calculate

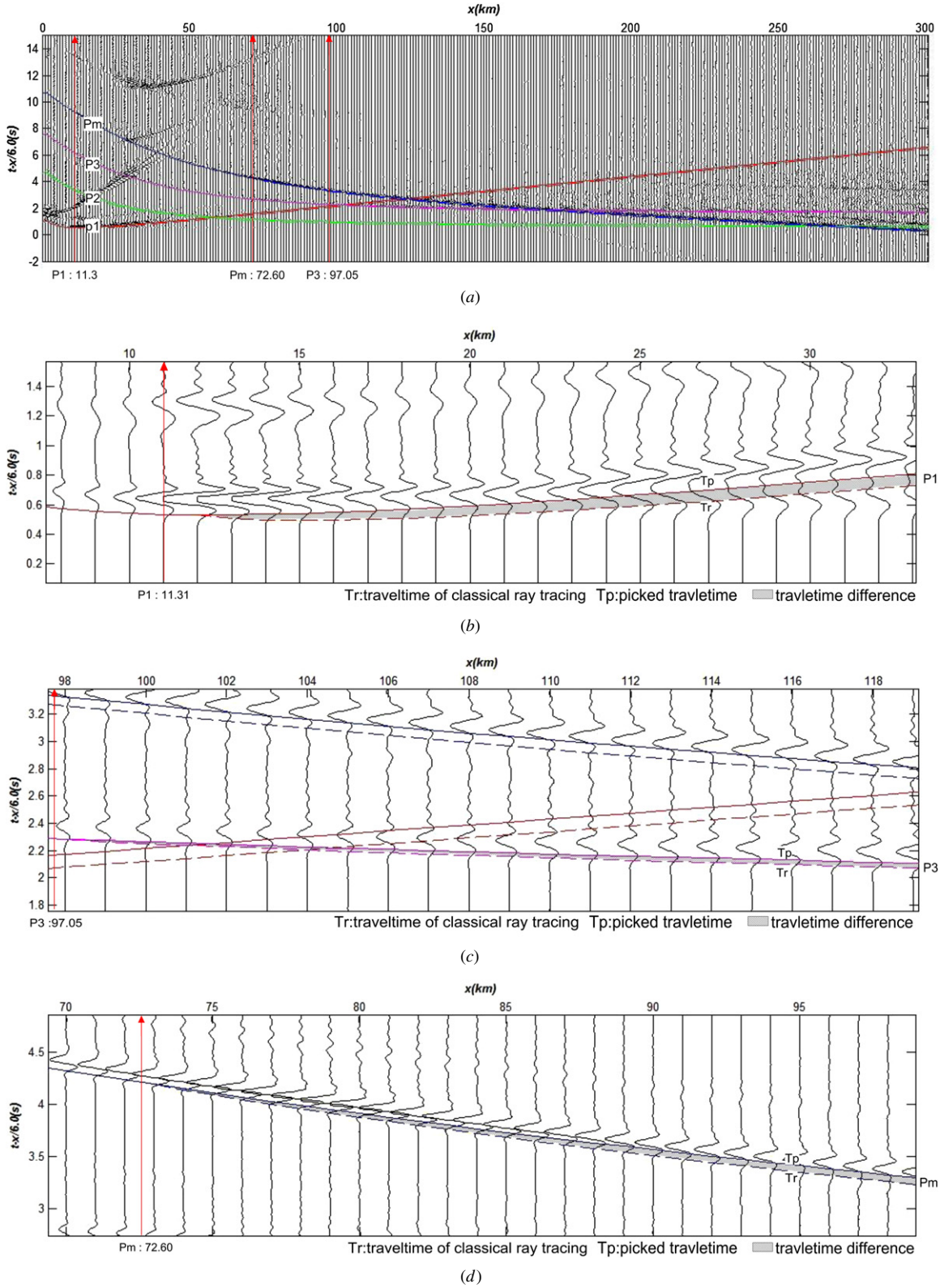

Figure 9. (*a*) The seismogram of horizontal components in the case of incident P wave and frequency 5 Hz. In the seismogram, we can observe the reflections of P1, P3 and Pm. The critical offsets of these reflections are shown. (*b*) The partly magnified diagram of P1 within the offset range of 8–26 km. There is travel-time difference (marked in hatching) between Tp (picked travel-time, marked in real curves) and Tr (travel-time of reflections calculated with classical ray tracing, marked in real curves) when the offset is 11.3 km. (*c*) The partly magnified diagram of P3 within the offset range of 95–120 km. There is travel-time difference when the offset is 94.3 km. (*d*) The partly magnified diagram of Pm within the offset range of 70–90 km. There is travel-time difference when the offset is 94.3 km.

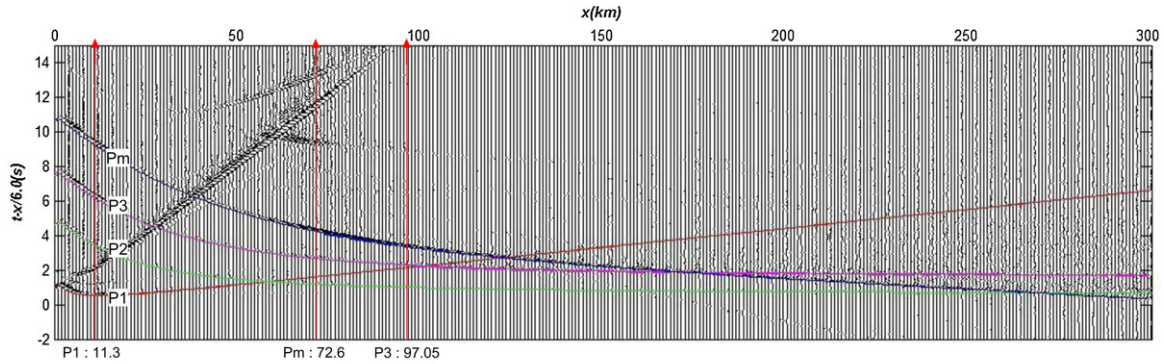

(*a*)

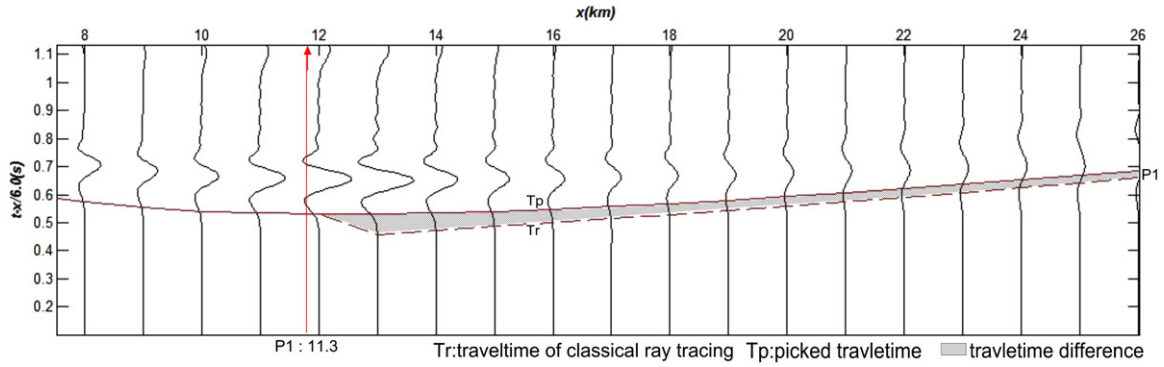

(*b*)

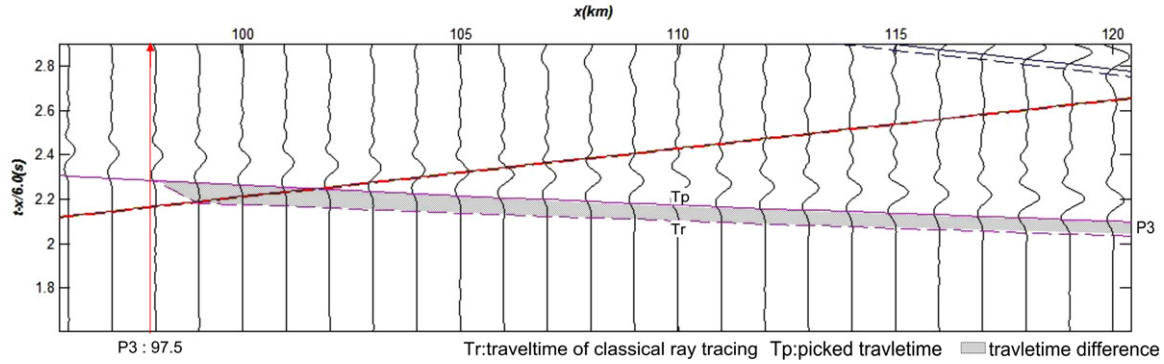

(*c*)

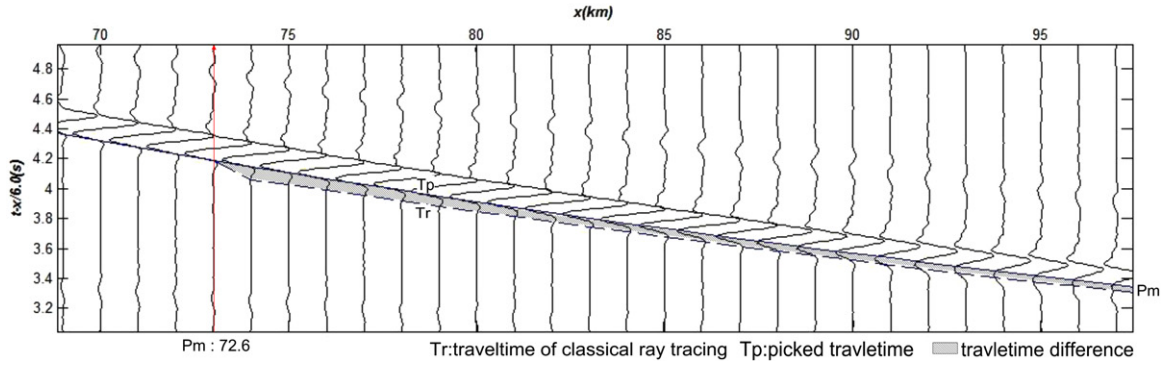

(*d*)

Figure 10. Same as figure 9, but for vertical components.

travel-times Tr (marked with dashed curves) of these reflections with the classical ray tracing technique (Cerveny and Firbas *et al* 1984). By comparing travel-times Tp and Tr in figures 9 and 10, we can observe their travel-time difference which is a result of wide-angle phase shift. Tp differs from Tr when the offset is larger than 11.3 km for reflection P1 from the sediment bottom, 94.3 km for the third reflection P3 and 71.2 km for the Moho reflection Pm. The travel-time difference

between Tp and Tr can be observed within the offset range of 8–26 km for P1 event, 95–120 km for P3 event and 70–90 km for PmP event (the details can be seen in figures 9(*b*)–(*d*) and 10(*b*)–(*d*)). For the given model, the phase shifts of the wide-angle seismic events P1, P3 and PmP are calculated with our approximate formulae. The calculated time shifts, shown in figures 7(*c*) and 8(*c*), are exactly well approached to the observed travel-time difference between Tp and Tr shown in figures 9 and 10. Summing up the time shifts (computed by our approximation formulae) and the ray traced travel-times, the results well match the picked travel-times, which highlights the efficiency of wide-angle seismic time-shift (phase-shift) correction in the interpretation of deep seismic sounding data, in which crustal thickness or crustal velocity is conventionally over- or underestimated (with neglect of the wide-angle effect).

5. Conclusion remarks

We present the approximation formula of time shift (phase shift) for post-critical incidence angles, with Taylor expansion of the ray parameter and horizontal slowness in the exact R/T equations (Aki and Richards 1980). Here explicit formulae of the reflection/transmission strength and time shift for post-critical incidence are obtained and their accuracies in approximation are evaluated through numerical experiments with comparisons of the wide-angle effects calculated with our approximation scheme, the exact ones (Aki and Richards 1980) and those computed with Downton's method (Downton and Ursenbach 2006). The comparison results demonstrate that (1) the precision is high for our approximation scheme of wide-angle seismic reflection, and (2) the wide-angle effect can be approximated with higher precision by fourth-order Taylor expansion than by second-order Taylor expansion in ray parameter and horizontal slowness.

Acknowledgments

We would like to thank F Li, H Lan and K Liang for their constructive comments. This study was financially supported by National Natural Science Foundation of China (41074033 and 41021063), the Ministry of Science and Technology and the Ministry of the Land and Resources (Sinoprobe-02-02 and 201111041).

Appendix A. Derivation of approximate expressions for all coefficients, R_{PP}, R_{PS}, T_{PP} and T_{PS} (situation 1)

Some variables made repeated use of are as follows:

$$a=\frac{V_{p1}}{V_{p2}},\quad b=\sqrt{1-\frac{V_{p1}^2}{V_{p2}^2}},\quad c=\frac{V_{s1}}{V_{p1}},$$
$$d=\frac{V_{s2}}{V_{p1}},\quad e=\frac{V_{s2}}{V_{p2}},\quad g=\sqrt{1-\frac{V_{p1}^2}{V_{s2}^2}}. \tag{A.1}$$

We start our work with the exact R/T coefficient formulae given by Aki and Richards (1980), as is shown in equation (1).

For the ray parameters and horizontal slowness, we make fourth-order Taylor expansions as

$$\begin{aligned}p&=\delta_1+\delta_2(\Delta\theta)+\delta_3(\Delta\theta)^2+\delta_4(\Delta\theta)^3+\delta_5(\Delta\theta)^4,\\ p^2&=\alpha_1+\alpha_2(\Delta\theta)+\alpha_3(\Delta\theta)^2+\alpha_4(\Delta\theta)^3+\alpha_5(\Delta\theta)^4,\\ p^4&=\beta_1+\beta_2(\Delta\theta)+\beta_3(\Delta\theta)^2+\beta_4(\Delta\theta)^3+\beta_5(\Delta\theta)^4,\\ p^6&=\gamma_1+\gamma_2(\Delta\theta)+\gamma_3(\Delta\theta)^2+\gamma_4(\Delta\theta)^3+\gamma_5(\Delta\theta)^4,\end{aligned} \tag{A.2}$$

$$\begin{aligned}q_{a1}&=A_0+B_0(\Delta\theta)+C_0(\Delta\theta)^2+D_0(\Delta\theta)^3+E_0(\Delta\theta)^4,\\ q_{b1}&=A_1+B_1(\Delta\theta)+C_1(\Delta\theta)^2+D_1(\Delta\theta)^3+E_1(\Delta\theta)^4,\end{aligned} \tag{A.3}$$

$$\begin{aligned}q_{b2}&=A_2+B_2(\Delta\theta)+C_2(\Delta\theta)^2+D_2(\Delta\theta)^3+E_2(\Delta\theta)^4,\\ q_{a2}&=-\mathrm{i}\sqrt{A_3+B_3(\Delta\theta)+C_3(\Delta\theta)^2+D_3(\Delta\theta)^3+E_3(\Delta\theta)^4}.\end{aligned} \tag{A.4}$$

Note that $\Delta\theta=\theta-e_c^p$, θ is the incident angle and e_c^p is the reflection PP critical angle. The coefficients of each expansion are

$$\begin{aligned}\delta_1&=\frac{a}{V_{p1}},\quad \delta_2=\frac{b}{V_{p1}},\quad \delta_3=\frac{-a}{2V_{p1}},\\ \delta_4&=-\frac{b}{6V_{p1}},\quad \delta_5=\frac{a}{24V_{p1}};\end{aligned} \tag{A.5}$$

$$\begin{aligned}\alpha_1&=\frac{a^2}{V_{p1}^2},\quad \alpha_2=\frac{2ab}{V_{p1}^2},\quad \alpha_3=\frac{1-2a^2}{V_{p1}^2},\\ \alpha_4&=-\frac{4ab}{3V_{p1}^2},\quad \alpha_5=\frac{2a^2-1}{3V_{p1}^2};\end{aligned} \tag{A.6}$$

$$\begin{aligned}\beta_1&=\frac{a^4}{V_{p1}^4},\quad \beta_2=\frac{4a^3b}{V_{p1}^4},\quad \beta_3=\frac{6a^2-8a^4}{V_{p1}^4},\\ \beta_4&=\frac{4(3ab-8a^3b)}{3V_{p1}^4},\quad \beta_5=\frac{3(1-2a^2)-8(3a^2b^2-a^4)}{3V_{p1}^4};\end{aligned} \tag{A.7}$$

$$\begin{aligned}\gamma_1&=\frac{a^6}{V_{p1}^6},\quad \gamma_2=\frac{6a^5b}{V_{p1}^6},\\ \gamma_3&=\frac{15a^4-18a^6}{V_{p1}^6},\quad \gamma_4=\frac{4(5a^3b-9a^5b)}{V_{p1}^6},\\ \gamma_5&=\frac{5(3a^2b^2-a^4)-9(5a^4b^2-a^6)}{V_{p1}^6};\end{aligned} \tag{A.8}$$

$$\begin{aligned}A_0&=\frac{b}{V_{p1}},\quad B_0=\frac{-a}{V_{p1}},\\ C_0&=\frac{-b}{2V_{p1}},\quad D_0=\frac{a}{6V_{p1}},\quad E_0=\frac{b}{24V_{p1}};\end{aligned} \tag{A.9}$$

$$\begin{aligned}A_1&=\frac{1}{V_{s1}}\sqrt{1-a^2c^2},\\ B_1&=-\frac{abc^2}{V_{s1}\sqrt{1-a^2c^2}},\\ C_1&=\frac{c^2(2a^2-1-a^4c^2)}{2V_{s1}(\sqrt{1-a^2c^2})^3},\end{aligned}$$

$$D_1 = \frac{1}{V_{s1}}\frac{abc^4(4-3c+3a^2c-5a^2c^2+a^4c^4)}{6(\sqrt{1-a^2c^2})^5},$$
$$E_1 = \frac{c^2(4-3c^2-8a^2+16a^2c^2-12a^2c^4-4a^4c^2+10a^4c^4-4a^6c^4+a^6c^6)}{24V_{s1}(\sqrt{1-a^2c^2})^7}; \tag{A.10}$$

$$A_2 = \frac{1}{V_{s1}}\sqrt{1-a^2d^2},$$
$$B_2 = -\frac{abd^2}{V_{s1}\sqrt{1-a^2d^2}},$$
$$C_2 = \frac{d^2(2a^2-1-a^4d^2)}{2V_{s1}(\sqrt{1-a^2d^2})^3},$$
$$D_2 = \frac{1}{V_{s1}}\frac{abd^4(4-3d+3a^2d-5a^2d^2+a^4d^4)}{6(\sqrt{1-a^2d^2})^5},$$
$$E_2 = \frac{d^2(4-3d^2-8a^2+16a^2d^2-12a^2d^4-4a^4d^2+10a^4d^4-4a^6d^4+a^6d^6)}{24V_{s1}(\sqrt{1-a^2d^2})^7}; \tag{A.11}$$

$$A_3 = 0, \quad B_3 = \frac{2ab}{V_{p1}^2}, \quad C_3 = \frac{1-2a^2}{V_{p1}^2},$$
$$D_3 = -\frac{4ab}{3V_{p1}^2}, \quad E_3 = \frac{2a^2-1}{3V_{p1}^2}. \tag{A.12}$$

Substituting equation (2) into equation (1), we can obtain the approximate formulae as

$$\begin{aligned} R_{\mathrm{PP}}(\theta) &\approx \frac{U_1(\theta)+\mathrm{i}U_2(\theta)}{O_1(\theta)+\mathrm{i}O_2(\theta)},\\ R_{\mathrm{PS}}(\theta) &\approx \frac{W_1(\theta)+\mathrm{i}W_2(\theta)}{O_1(\theta)+\mathrm{i}O_2(\theta)},\\ T_{\mathrm{PS}}(\theta) &\approx \frac{X_1(\theta)+\mathrm{i}X_2(\theta)}{O_1(\theta)+\mathrm{i}O_2(\theta)},\\ T_{\mathrm{PP}}(\theta) &\approx \frac{V(\theta)}{O_1(\theta)+\mathrm{i}O_2(\theta)}. \end{aligned} \tag{A.13}$$

The expansion terms of equation (3) are as follows:

$$\begin{aligned} U_1(\theta) &= U_{11}+U_{12}(\theta-e_c^p)+U_{13}(\theta-e_c^p)^2\\ &\quad +U_{14}(\theta-e_c^p)^3+U_{15}(\theta-e_c^p)^4,\\ U_2(\theta) &= [U_{21}+U_{22}(\theta-e_c^p)+U_{23}(\theta-e_c^p)^2\\ &\quad +U_{24}(\theta-e_c^p)^3+U_{25}(\theta-e_c^p)^4]Q_2,\\ O_1(\theta) &= O_{11}+O_{12}(\theta-e_c^p)+O_{13}(\theta-e_c^p)^2\\ &\quad +O_{14}(\theta-e_c^p)^3+O_{15}(\theta-e_c^p)^4,\\ O_2(\theta) &= [O_{21}+O_{22}(\theta-e_c^p)+O_{23}(\theta-e_c^p)^2\\ &\quad +O_{24}(\theta-e_c^p)^3+O_{25}(\theta-e_c^p)^4]Q_2,\\ W_1(\theta) &= W_{11}+W_{12}(\theta-e_c^p)+W_{13}(\theta-e_c^p)^2\\ &\quad +W_{14}(\theta-e_c^p)^3+W_{15}(\theta-e_c^p)^4,\\ W_2(\theta) &= [W_{21}+W_{22}(\theta-e_c^p)+W_{23}(\theta-e_c^p)^2\\ &\quad +W_{24}(\theta-e_c^p)^3+W_{25}(\theta-e_c^p)^4]Q_2,\\ X_1(\theta) &= X_{11}+X_{12}(\theta-e_c^p)+X_{13}(\theta-e_c^p)^2\\ &\quad +X_{14}(\theta-e_c^p)^3+X_{15}(\theta-e_c^p)^4,\\ X_2(\theta) &= [X_{21}+X_{22}(\theta-e_c^p)+X_{23}(\theta-e_c^p)^2\\ &\quad +X_{24}(\theta-e_c^p)^3+X_{25}(\theta-e_c^p)^4]Q_2,\\ V(\theta) &= V_{11}+V_{12}(\theta-e_c^p)+V_{13}(\theta-e_c^p)^2\\ &\quad +V_{14}(\theta-e_c^p)^3+V_{15}(\theta-e_c^p)^4. \end{aligned} \tag{A.14}$$

Here the detailed expressions are not given because of space limitations; they can be obtained by contacting the corresponding author.

Appendix B. Derivation of approximate expressions for all coefficients, R_{PP}, R_{PS}, T_{PP} and T_{PS} (situation 2)

The derivation in situation 2 is similar to that in situation 1.

The approximate expressions are similar to those in equation (3), but for T_{PP} it is

$$T_{\mathrm{PP}}(\theta) \approx \frac{V_1(\theta)+\mathrm{i}V_2(\theta)}{O_1(\theta)+\mathrm{i}O_2(\theta)}. \tag{B.1}$$

The used expressions and variables are as follows:

$$\begin{aligned} O_1 &= [O_{11}+O_{12}(\theta-e_c^s)+O_{13}(\theta-e_c^s)^2+O_{14}(\theta-e_c^s)^3\\ &\quad +O_{15}(\theta-e_c^s)^4]+[O_{21}+O_{22}(\theta-e_c^s)+O_{23}(\theta-e_c^s)^2\\ &\quad +O_{24}(\theta-e_c^s)^3+O_{25}(\theta-e_c^s)^4]Q_{2p}Q_{2s},\\ O_2 &= Q_{2p}[O_{31}+O_{32}(\theta-e_c^s)+O_{33}(\theta-e_c^s)^2+O_{34}(\theta-e_c^s)^3\\ &\quad +O_{35}(\theta-e_c^s)^4]+Q_{2s}[O_{41}+O_{42}(\theta-e_c^s)\\ &\quad +O_{43}(\theta-e_c^s)^2+O_{44}(\theta-e_c^s)^3+O_{45}(\theta-e_c^s)^4]Q_{2p}Q_{2s}, \end{aligned} \tag{B.2}$$

$$\begin{aligned} U_1 &= [U_{11}+U_{12}(\theta-e_c^s)+U_{13}(\theta-e_c^s)^2+U_{14}(\theta-e_c^s)^3\\ &\quad +U_{15}(\theta-e_c^s)^4]+[U_{21}+U_{22}(\theta-e_c^s)+U_{23}(\theta-e_c^s)^2\\ &\quad +U_{24}(\theta-e_c^s)^3+U_{25}(\theta-e_c^s)^4]Q_{2p}Q_{2s},\\ U_2 &= Q_{2p}[U_{31}+U_{32}(\theta-e_c^s)+U_{33}(\theta-e_c^s)^2+U_{34}(\theta-e_c^s)^3\\ &\quad +U_{35}(\theta-e_c^s)^4]+Q_{2s}[U_{41}+U_{42}(\theta-e_c^s)\\ &\quad +U_{43}(\theta-e_c^s)^2+U_{44}(\theta-e_c^s)^3+U_{45}(\theta-e_c^s)^4], \end{aligned} \tag{B.3}$$

$$\begin{aligned} W &= [W_{11}+W_{12}(\theta-e_c^s)+W_{13}(\theta-e_c^s)^2+W_{14}(\theta-e_c^s)^3\\ &\quad +W_{15}(\theta-e_c^s)^4]+[W_{21}+W_{22}(\theta-e_c^s)+W_{23}(\theta-e_c^s)^2\\ &\quad +W_{24}(\theta-e_c^s)^3+W_{25}(\theta-e_c^s)^4]Q_{2p}Q_{2s}, \end{aligned} \tag{B.4}$$

$$\begin{aligned} X_1 &= [X_{11}+X_{12}(\theta-e_c^s)+X_{13}(\theta-e_c^s)^2\\ &\quad +X_{14}(\theta-e_c^s)^3+X_{15}(\theta-e_c^s)^4],\\ X_2 &= [X_{21}+X_{22}(\theta-e_c^s)+X_{23}(\theta-e_c^s)^2\\ &\quad +X_{24}(\theta-e_c^s)^3+X_{25}(\theta-e_c^s)^4]Q_{2p}, \end{aligned} \tag{B.5}$$

$$\begin{aligned} V_1 &= [V_{11}+V_{12}(\theta-e_c^s)+V_{13}(\theta-e_c^s)^2\\ &\quad +V_{14}(\theta-e_c^s)^3+V_{15}(\theta-e_c^s)^4],\\ V_2 &= [V_{21}+V_{22}(\theta-e_c^s)+V_{23}(\theta-e_c^s)^2\\ &\quad +V_{24}(\theta-e_c^s)^3+V_{25}(\theta-e_c^s)^4]Q_{2s}. \end{aligned} \tag{B.6}$$

Appendix C. New approximate formulae for reflection and transmission of plane seismic waves

If the frequency of the incident seismic wave is f, we can obtain the strength approximation formula for the reflective PS wave,

$$|R_{\mathrm{PS}}(\theta)| = \frac{\sqrt{(W_1O_1 + W_2O_2)^2 + (W_2O_1 - W_1O_2)^2}}{O_1^2 + O_2^2}, \quad \text{(C.1)}$$

and the time shift,

$$\Delta t = \frac{\varphi}{2\pi f}, \quad \text{(C.2)}$$

where

$$\varphi(\theta) = \arctan\left(\frac{W_2O_1 - W_1O_2}{W_1O_1 + W_2O_2}\right). \quad \text{(C.3)}$$

For the transmissive PP wave, the strength is

$$|T_{\mathrm{PP}}(\theta)| = \frac{\sqrt{(V_1O_1 + V_2O_2)^2 + (V_2O_1 - V_1O_2)^2}}{O_1^2 + O_2^2}, \quad \text{(C.4)}$$

and the time shift (the frequency of incident seismic wave is f) is

$$\Delta t = \frac{\varphi}{2\pi f}, \quad \text{(C.5)}$$

where

$$\varphi(\theta) = \arctan\left(\frac{V_2O_1 - V_1O_2}{V_1O_1 + V_2O_2}\right). \quad \text{(C.6)}$$

For the transmissive PS wave, the strength is

$$|T_{\mathrm{PS}}(\theta)| = \frac{\sqrt{(X_1O_1 + X_2O_2)^2 + (X_2O_1 - X_1O_2)^2}}{O_1^2 + O_2^2}, \quad \text{(C.7)}$$

and the time shift (the frequency of incident seismic wave is f) is

$$\Delta t = \frac{\varphi}{2\pi f}, \quad \text{(C.8)}$$

where

$$\varphi(\theta) = \arctan\left(\frac{X_2O_1 - X_1O_2}{X_1O_1 + X_2O_2}\right). \quad \text{(C.9)}$$

Expressions for O_1, O_2, W_1, W_2, V_1, V_2, X_1, X_2 are shown in appendices A and B, respectively, corresponding to situations 1 and 2.

References

Aki K and Richards P 1980 *Quantitative Seismology—Theory and Method* (San Francisco, CA: Freeman)

Bortfeld R 1961 Approximation to the reflection and transmission coefficients of plane longitudinal and transverse waves *Geophys. Prospect.* **9** 485–502

Carpenter M A 2006 Elastic properties of minerals and the influence of phase transitions *Am. Mineral.* **91** 229–46

Cerveny V and Firbas P 1984 Numerical modelling and inversion of travel times of seismic body waves in inhomogeneous anisotropic media *Geophys. J. R. Astron. Soc.* **76** 41–51

Downton J E and Ursenbach C 2006 Linearized amplitude variation with offset (AVO) inversion with supercritical angles *Geophysics* **71** 49–55

Lan H Q and Zhang Z J 2011a Comparative study of the free-surface boundary condition in two-dimensional finite-difference elastic wave field simulation *J. Geophys. Eng.* **8** 275–86

Lan H Q and Zhang Z J 2011b Three-dimensional wave-field simulation in heterogeneous transversely isotropic medium with irregular free surface *Bull. Seismol. Soc. Am.* **101** 1354–70

Li S L and Mooney W D 1998 Crustal structure of China from deep seismic sounding profiles *Tectonophysics* **288** 105–13

Makovsky Y, Klemperer S L, Ratschbacher L, Brown L D, Li M and Zhao W J 1996 INDEPTH wide-angle reflection observation of P-wave-to-S-wave conversion from crustal bright spots in Tibet *Science* **274** 1690–1

Mallick S 1993 A simple approximation to the P-wave reflection coefficient and its implication in the inversion of amplitude variation with offset data *Geophysics* **58** 544–52

Oliver G J H and Coggon J H 1979 Crustal structure of Fiordland, New Zealand *Tectonophysics* **54** 253

Oueity J and Clowes R M 2010 Nature of the Moho transition in NW Canada from combined near-vertical and wide-angle seismic-reflection studies *Geophys. J. R. Astron. Soc.* **2** 377–96

Pramanik A G, Painuly P K, Singh V and Katiyar R 2001 Geophysical technology integration in hydrocarbon exploration and production: an overview *Geohorizons* **6** 15–34

Richards P G and Frasier C W 1976 Scattering of elastic waves from depth-dependent inhomogeneities *Geophysics* **41** 441–58

Shuey R T 1985 A simplification of the Zoeppritz equations *Geophysics* **50** 609–14

Ursenbach C P 2003a Testing pseudo-linear Zoeppritz approximations: P wave AVO inversion *CREWES Res. Rep.* **15** 13–27

Ursenbach C P 2003b Testing pseudo-linear Zoeppritz approximations: multicomponent and joint AVO inversion *Crewes Res. Rep.* **15** 1–12

Virieux J 1984 SH-velocity-stress finite-difference method: velocity-stress finite-difference method *Geophysics* **49** 1933–57

Wang Y H 1999 Approximations to the Zoeppritz equations and their use in AVO analysis *Geophysics* **64** 1920–7

Wiggins R, Kenny G S and McClure C D 1984 A method for determining and displaying the shear-velocity reflectivities of a geologic formation *European Patent* application 0113944

Zhang Z J, Deng Y F, Teng J W, Wang C Y, Gao R, Chen Y and Fan W M 2011a An overview of the crustal structure of the Tibetan plateau after 35 years of deep seismic soundings *J. Asian Earth Sci.* **40** 977–89

Zhang Z J, Yang L Q, Teng J W and Badal J 2011b An overview of the earth crust under China *Earth Sci. Rev.* **104** 143–66